ARTICLES

The formation and expansion of a toroidal drop moving in a viscous fluid

Masami Kojima,[a] E. J. Hinch,[b] and Andreas Acrivos
Department of Chemical Engineering, Stanford University, Stanford, California 94305

(Received 27 July 1983; accepted 14 September 1983)

The deformation of an initially spherical liquid drop moving under the action of gravity in another fluid with which it is completely miscible is investigated under conditions of small values of the drop Reynolds number. It is found experimentally that such a drop evolves into an open torus which subsequently expands, and this phenomenon is examined theoretically for two limiting drop geometries: (i) a slightly deformed spherical drop, and (ii) a highly expanded, slender open torus. Under the assumptions of zero interfacial tension and creeping flow, the theory provides a qualitative description for the initial stages of the drop evolution [case (i)], but is unable to account for the observed drop expansion during latter stages of deformation [case (ii)]. On the other hand, if small inertial effects are retained in the analysis, the theory predicts that a slender open fluid torus possessing an arbitrary cross-sectional geometry will expand without change of shape to first order in Reynolds number. Quantitative comparisons of theoretically predicted rates of expansion with experimental measurements suggest the possible existence of a small, time-dependent interfacial tension across the drop interface.

I. INTRODUCTION

There exists evidence in the literature that, at low Reynolds numbers, an aggregate of microscopically small particles suspended in a viscous fluid exhibits a behavior similar to that of a drop with negligible interfacial tension under certain restricted conditions. The experimental work of Powell and Mason,[1] who studied the breakup of aggregates in linear shear flows, provides such an example. These authors formed small spherical aggregates by suspending clusters of neutrally buoyant polystyrene beads in the ambient viscous liquid. They then observed that, in a simple shear flow, such an aggregate, with solids' volume fraction no higher than 55%, underwent a periodic extension and compression similar to that found when a liquid having negligible interfacial tension but a viscosity much larger than that of the bulk medium is sheared under similar flow conditions.[2,3]

It was demonstrated in our laboratory that when an aggregate, whose structure was as described above and whose density differed from that of the surrounding liquid, was allowed to fall freely under the force of gravity at small Reynolds numbers, it deformed into a ring-like shape which subsequently expanded before it eventually disintegrated. Furthermore, when the experiment was repeated with viscous miscible drops, the same pattern was observed. To the authors' knowledge, despite extensive studies reported in the literature on vortex rings in high Reynolds number flows, no mention has been made to date of a corresponding toroidal drop formation at low Reynolds numbers. Thus an analytical examination of the deformation of such viscous drops is of interest in its own right, and in addition may augment our present understanding of aggregate breakup.

In what follows, we shall present a theoretical investigation of spherical and toroidal drops falling at small Reynolds numbers which we shall then test by comparing the theoretical predictions with results of experiments performed with falling viscous drops that were miscible with the ambient liquid. We shall first summarize certain experimental observations in our laboratory pertaining to the deformation of such drops and defer until Sec. V of this paper a more detailed description of the experiments.

The fluids were prepared from mixtures of light corn syrup and water having different compositions, and the mixture with a higher viscosity and density was dyed. Colored drops were formed outside the vessel which contained the fluid with the lower density, and were released from just above the free interface. The primary features of the subsequent evolution of the drop contour were as follows.

(1) As the drop entered the bulk medium, a tail emanated from the rear stagnation point which became increasingly thinner with time as the drop continued to fall (Fig. 1).

(2) The region near the rear stagnation point of the drop flattened and eventually formed a depression which deepened around the axis of symmetry of the drop (Fig. 2). In time, the tail was cut off and the drop in turn deformed into a shape resembling a torus (Fig. 3).

(3) The toroidal drop expanded and became slender as it continued to fall. Eventually, however, instabilities set in and the drop broke up (Fig. 4).

Our analysis will deal separately with the initial and final stages of drop deformation in which the drop shape will be approximated by, respectively, a slightly deformed sphere and an open torus. At first inertial effects will be assumed to be negligible everywhere, but time-dependent kinematics as well as a finite interfacial tension will be included in the theoretical development. It will be shown that, under conditions of creeping flow and zero interfacial tension, the analysis predicts the formation and the subsequent deepening of a

[a] Present address: Department of Chemical Engineering, The University of Capetown, Rondebosch, C.P. 7700, South Africa.
[b] Present address: Department of Applied Mathematics and Theoretical Physics, Cambridge, England.

 0031-9171/84/010019-14$01.90

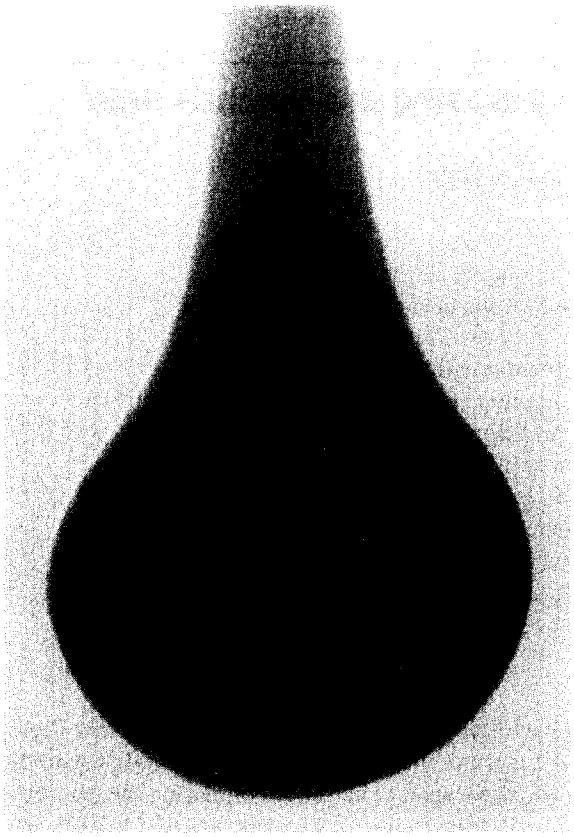

FIG. 1. Sideview photograph of a viscous drop entering the bulk medium. Drop composition: corn syrup–water mixture of viscosity 3.9 P and density 1.329 g/cm^3; bulk medium composition: corn syrup–water mixture of viscosity 0.51 P and density 1.264 g/cm^3.

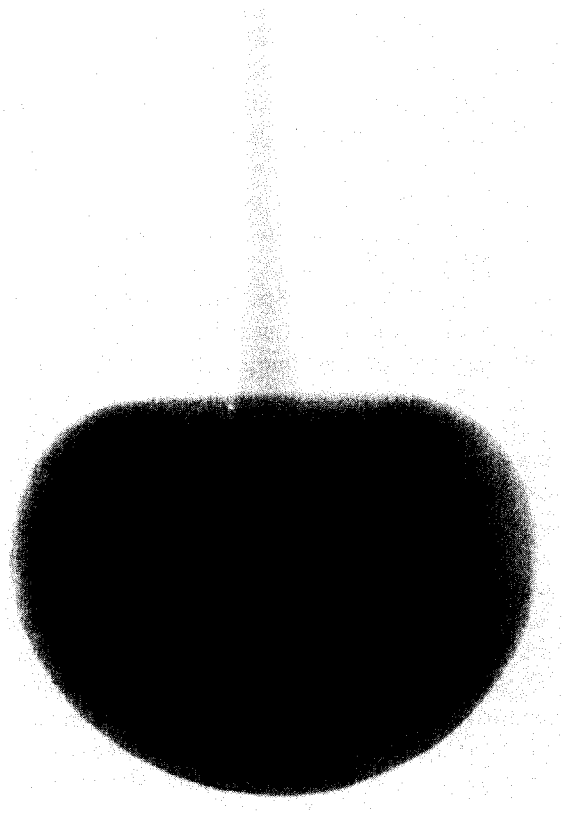

FIG. 2. Sideview photograph of a viscous drop with a depression forming at the rear stagnation point; same fluid compositions as in Fig. 1.

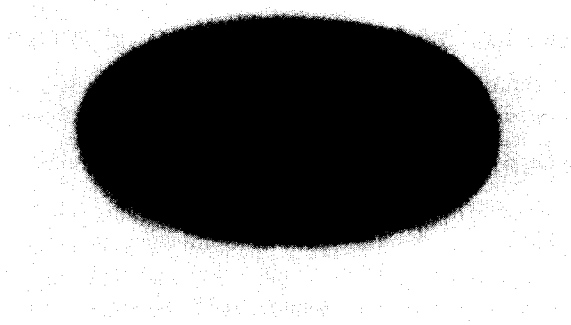

FIG. 3. Photograph of a newly formed ring; same fluid compositions as in Fig. 1.

depression near the rear stagnation point of a slightly deformed fluid sphere if an appropriate initial drop geometry is assumed. However, in the case of a highly expanded fluid ring, the theory leads to the conclusion that even though drops with certain initial configurations will expand for a finite time interval, such an expansion must eventually cease and be followed by a drop contraction. Clearly, a creeping flow analysis is inadequate to explain the experimental findings, and thus we shall consider next the influence of small inertia on the drop deformation. It will be shown that the leading-order Reynolds number correction indeed induces the expansion of a toroidal drop with arbitrary cross-sectional geometry without change of shape, but at a rate consistently above that measured experimentally if the interfacial tension is taken to be negligibly small. We offer, as a possible explanation of this discrepancy between theory and experiment, the notion that, in any experimental setup such as ours, there exists a finite transient interfacial tension across the interface between two miscible liquids which impedes the expansion of fluid rings.

II. NEARLY SPHERICAL DROPS

Consider the motion of a nearly spherical, viscous drop falling freely under the force of gravity in an unbounded, quiescent fluid at low Reynolds number. We assume that

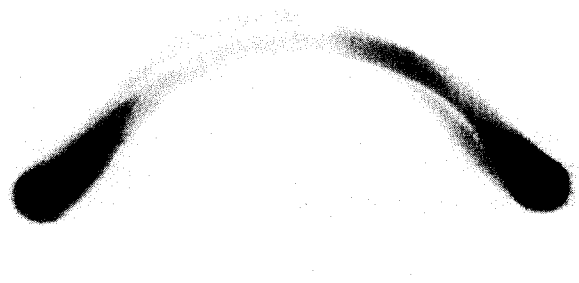

FIG. 4. Photograph of the breakup of a ring; same fluid compositions as in Fig. 1.

both fluids are incompressible and that the flow is axisymmetric everywhere. We fix the origin at the center of the mass of the drop, and designate all quantities inside the drop by a caret. We render the equations and boundary conditions dimensionless in the usual manner using a, the radius of the "equivalent" or undeformed spherical drop, as the characteristic length scale and U, the settling speed of the drop, as the characteristic velocity; in addition, we nondimensionalize the stresses with respect to $\mu U/a$, where μ is the viscosity of the external fluid and define the Reynolds number $\mathrm{Re} \equiv a\rho U/\mu$, where ρ is the density of the ambient fluid. We seek to solve the equations of motion, which in view of the axisymmetry of the flow can be expressed in terms of the stream functions ψ and $\hat{\psi}$, subject to the boundary conditions of continuity of velocity and shear stress across the drop surface, and a jump in the normal stress equal to $N\nabla \cdot \mathbf{n}$, where $\mathbf{n}$ is the unit outward vector normal to the surface and N is the inverse capillary number, $N = \gamma/\mu U$, with γ being the interfacial tension. We also require that the velocity become uniform far away from the drop. Owing to the fact that a torus formation was observed at Reynolds numbers as low as 7×10^{-3}, we begin our analysis by neglecting inertial effects everywhere.

A. Steady Stokes solutions

If, in the above formulation, the normal component of the velocity is set equal to zero at the drop interface, the resulting and well-known Hadamard–Rybczynski solution[4] can be shown to satisfy exactly all the steady-state boundary conditions on the surface of a fluid sphere for all values of N. Thus, the sphere represents one possible steady shape for the drop under creeping flow conditions.

It is interesting to examine, however, whether other possibilities can exist in the absence of inertial effects. Taylor and Acrivos[4] and Matunobu[5] confined their attention to the case in which the sphere is slightly deformed and set

$$r \equiv R(\theta) = 1 + g(\theta), \quad \max|g(\theta)| \ll 1,$$

where r is the radial distance from the origin and θ is the polar angle measured from the rear stagnation point. Taylor and Acrivos[4] took the interfacial tension to be large such that $N\nabla \cdot \mathbf{n} \sim O(1)$, and showed that the sphere is the only possible steady shape if $|g(\theta)| \ll 1$. On the other hand, Matunobu[5] considered the case $N\nabla \cdot \mathbf{n} \ll 1$ and, after introducing the small perturbation parameter to be denoted here by $\delta \ll 1$, expanded the equation for the surface of the drop in powers of δ,

$$R(\theta) = 1 + \delta \sum_{n=2}^{\infty} (2n+1) f_n P_n(\cos\theta) + O(\delta^2), \qquad (1)$$

where P_n are the Legendre polynomials of order n. The absence of the terms P_0 and P_1 in Eq. (1) insures that volume is conserved and that the origin remains at the center of mass of the drop.

Matunobu[5] carried out the algebra to $O(\delta)$ and obtained a set of equations whose solution left f_2 arbitrary in that all the succeeding f_n's could in turn be determined by solving his difference equation (4.16). He thus concluded that there existed a single continuous family of steady configurations and that the nature of the deviation from the spherical shape, i.e., the sign of f_2, was arbitrary.

The explanation for this seemingly paradoxical nature of Matunobu's result, paradoxical especially since δ cannot be related to any physical parameter of the system, becomes apparent upon a careful examination of his equation (4.16) which, when modified for a falling drop, has the asymptotic form, as $n \to \infty$,

$$f_{n+1} + 2Nf_n - f_{n-1} \sim 0. \qquad (2)$$

On solving Eq. (2), we obtain for the ratio of two successive terms,

$$f_{n+1}/f_n = -N \pm (N^2+1)^{1/2}.$$

That the actual equation gives $-N-(N^2+1)^{1/2}$ for this ratio can be seen by noting that, for all $n \geqslant 2$, Matunobu's equation (4.16) for a falling drop gives

$$f_{n+1} = -Nh_n f_n + h'_n f_{n-1},$$

where both h_n and h'_n are positive functions of n and of the ratio of the viscosities in the two phases; hence, since $f_1 = 0$ and f_2 is arbitrary, all the succeeding f_n's alternate in sign. For $N \neq 0$, the resulting series then clearly diverges at $\theta = \pi$ and possibly for other values of θ as well. Furthermore, if $N = 0$, we first observe that, since the coefficients of all the odd P_n's are zero, the series reduces to $\Sigma_{n=1}^{\infty} (4n+1) f_{2n} P_{2n}(\cos\theta)$, which once again diverges since, at large n, $f_{n+1} \sim f_{n-1}$. It therefore follows that all the steady solutions derived by Matunobu are invalid except, of course, for $f_n = 0$.

B. Time-dependent kinematics

We shall next consider the evolution in time of a spherical drop subject to small perturbations. The method of solution is identical to that employed in the preceding subsection with the modification that the equation for the drop surface is now time-dependent. Thus the boundary condition for the normal component of the velocity is given by

$$\mathbf{u} \cdot \mathbf{n} = \hat{\mathbf{u}} \cdot \mathbf{n} = \frac{(a/U)(\partial R/\partial t^*)}{|\mathbf{i}_r - \nabla R|}, \qquad (3)$$

where t^* is dimensional, and $\mathbf{i}_r$ is a unit outwad vector in the radial direction. We perturb the spherical shape by setting one of the f_n's to a nonzero constant at $t^* = 0$ and follow the deformation of the drop. Of course, the result is readily generalized to an arbitrary initial perturbation by means of superposition. We note that, in contrast to the steady-state case discussed in the previous section, δ, being a measure of the initial deformation imposed on the drop, is now a well-defined physical parameter for the entire range of N. The implementation of the boundary condition (3) then yields a set of coupled differential equations for f_n, shown here for a falling drop,

$$G_n \frac{a}{U}\frac{df_n}{dt^*} = -H_n f_{n+1} - Q_n f_n + W_n f_{n-1}, \quad n \geqslant 2, \quad (4)$$

$$G_n = \frac{2(\lambda+1)(2n+1)}{n(n+1)}[(4n^4+8n^3+2n^2-8n-6)\lambda^2 + (8n^4+16n^3+4n^2-4n+3)\lambda + (4n^4+8n^3+2n^2+4n)],$$

$$H_n = (4n^4+8n^3+14n^2+10n+9)\lambda^2 + (8n^4+16n^3+34n^2-40n-27)\lambda + (4n^4+8n^3+20n^2+22n+18),$$

$$Q_n = 2N(\lambda+1)^2(2n+1)^2(n-1)(n+2),$$

$$W_n = 2(\lambda+1)(n+2)(n-2)[(2n^2+4n+3)\lambda + (2n^2+4n)],$$

where $\lambda \equiv \hat{\mu}/\mu$ with $\hat{\mu}$ being the viscosity of the fluid within the drop. As expected, at steady state, Eq. (4) reduces to Matunobu's equation (4.16) for a falling drop. When $N \gg 1$, which corresponds to the high interfacial tension limit, these equations simplify to

$$G_n \frac{a}{U}\frac{df_n}{dt^*} = -Q_n f_n, \quad (5)$$

from which it is immediately apparent that any deviation from a spherical shape decays exponentially in time, with characteristic time $a\mu/\gamma$ if λ is $O(1)$.

When N is of $O(1)$, t^* should be rendered dimensionless with respect to a/U, so that $t = t^* U/a$, and the full system (4) must be solved. Recast in matrix formulation, Eq. (4) becomes

$$\frac{d}{dt}\mathbf{f} = \mathsf{A}\,\mathbf{f}, \quad (6)$$

where A is the semiinfinite tridiagonal matrix

$$\mathsf{A} = \begin{pmatrix} -Q_2/G_2 & -H_2/G_2 & 0 & \cdot & \cdot \\ W_3/G_3 & -Q_3/G_3 & -H_3/G_3 & 0 & \cdot \\ 0 & W_4/G_4 & -Q_4/G_4 & \cdot & \cdot \\ 0 & 0 & W_5/G_5 & \cdot & \cdot \\ \cdot & \cdot & \cdot & \cdot & \cdot \end{pmatrix},$$

and f is a semi-infinite vector whose elements are f_n. As before, for our solution to remain valid, we require that the series $\Sigma_{n=2}^{\infty}(2n+1)f_n P_n(\cos\theta)$ converge for all time and θ. We thus truncate f to a finite M vector,

$$\frac{d}{dt}\mathbf{f}_M = \mathsf{A}_M\,\mathbf{f}_M, \quad (7)$$

where A_M is an $M \times M$ submatrix of A, and then check the validity of our solution *a posteriori* by testing the convergence of the series as obtained from the solution of Eq. (7). We first note that the temporal stability of the spherical drop is determined by the signs of the real parts of the eigenvalues of A_M. It can be shown,[6] however, that all of these are zero if all the diagonal elements of A_M are zero, and that all are negative otherwise. But the diagonal elements of A vanish if and only if $N = 0$, and consequently, irrespective of the magnitude of M, all the eigenvalues of A_M have negative real parts for any nonzero N, however small. Before discussing the implications of this result in more detail, we shall consider first the case of zero interfacial tension.

Since γ was very small in the experiments, let us for a moment assume that the interfacial tension effects are negligible and set $N = 0$ so as to simplify the analysis. The asymptotic form of Eq. (4) as $n \to \infty$ then becomes

$$\frac{d}{dt}f_n = \frac{1}{2(1+\lambda)}\frac{n(n+1)}{(2n+1)}[f_{n-1} - f_{n+1} + O(n^{-2})]. \quad (8)$$

First of all, it is easy to show[7] from the form of Eq. (8) that the "spectrum" of the disturbance would be expected to evolve towards higher harmonics as t increases and thus that the series cannot be truncated at a given M for all time. This is evident from Table I, which shows the values of $f_n(t)$ obtained by numerically integrating Eq. (7) with the initial condition, $f_2(0) = -1$, $f_n(0) = 0$ $(n \neq 2)$, using a fourth-order Runge–Kutta scheme.

More importantly, it is instructive to examine Eq. (8) and, in particular, to compare its solutions with those of Eq. (7). Let $f \sim \Sigma_{n=1}^{\infty}(2n+1)f_n P_n(\cos\theta)$ which, according to Eq. (8), satisfies

$$\frac{\partial f}{\partial t} - \frac{1}{2(1+\lambda)}\sin\theta\frac{\partial f}{\partial \theta} = \frac{\cos\theta}{(1+\lambda)}f, \quad (9)$$

if the $O(n^{-2})$ terms are omitted. Of course, since the equation governing f is based on Eq. (8) which applies only as $n \to \infty$, solutions to Eq. (9) cannot yield quantitative information about the deformation of the drop surface. Another limitation of this asymptotic approach is that df_1/dt is not zero in Eq. (9) and hence the requirement that the origin remain fixed at the center of mass of the drop is not satisfied. Nevertheless, it is illuminating to study Eq. (9) and check whether its solutions are in qualitative agreement with the numerical solutions of Eq. (7). From Eq. (9), we find that f is given by

$$f(t) = f(0)\left(\frac{1+\cot^2\theta(t)/2}{1+\cot^2\theta(0)/2}\right)^2 \exp\left(\frac{-t}{1+\lambda}\right), \quad (10a)$$

along the characteristics

$$[\cot\theta(0)/2]\exp(\tfrac{1}{2}t/1+\lambda) = \cot\theta(t)/2. \quad (10b)$$

In order to interpret Eq. (10a), we first examine its right-hand side in the limit as $\theta(0) \to 0$ and $\theta(0) \to \pi$. If we let $\theta(0) \to 0$, we obtain

$$f(t) \to f(0)\exp(t/1+\lambda),$$

whereas in the opposite limiting case, $\theta(0) \to \pi$,

$$f(t) \to f(0)\exp(-t/1+\lambda).$$

Second, as seen from the characteristic curves drawn in Fig.

TABLE I. The Legendre coefficients obtained from numerically integrating Eq. (7) truncated at $M = 100$. $\lambda = 0.2$, $f_2(0) = -1$, and $f_n(0) = 0$ $(n \neq 2)$.

Ut^*/a	f_2	f_{20}	f_{60}
2	−0.52	-3×10^{-6}	-2.8×10^{-21}
4	−0.073	-1.6×10^{-2}	-5.3×10^{-8}
6	0.0014	−0.13	-3.2×10^{-3}

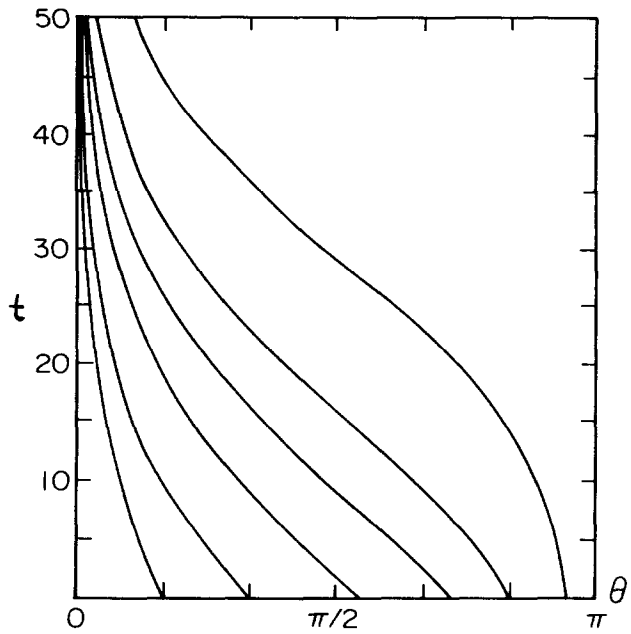

FIG. 5. The characteristics given by Eq. (10b) with $\lambda = 5$.

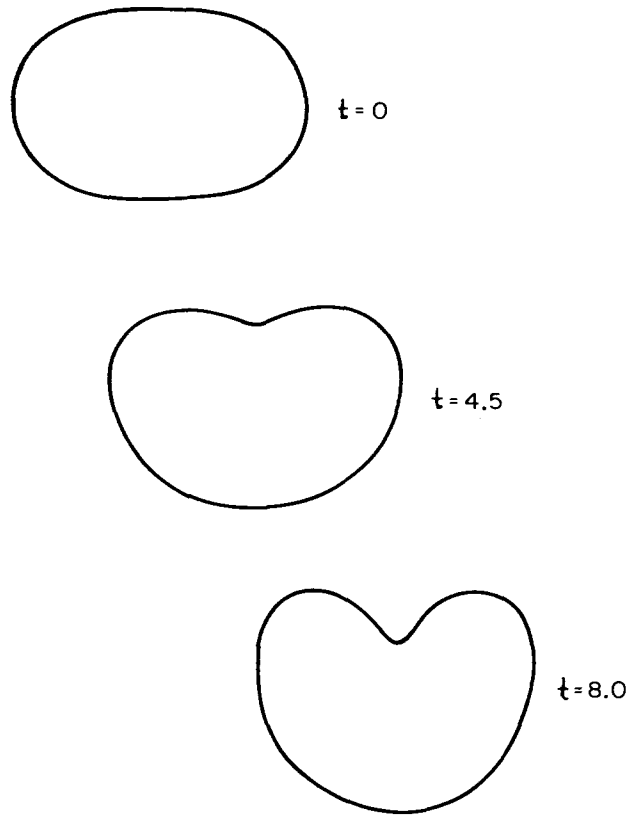

FIG. 6. Numerically obtained time-dependent deformation of an initially oblate spheroidal drop; $\lambda = 5$, $N = 0$, $\delta = 0.057$, $f_2(0) = -1$, and $f_n(0) = 0$ $(n \neq 2)$.

5, all the characteristics crossing the lines of constant t, as $t \to \infty$, emanate from the region $\theta(0) \sim \pi$, except near $\theta = 0$. In other words, f decays exponentially with time and the drop becomes spherical everywhere except in the neighborhood of its rear stagnation point, $\theta = 0$, where the initial disturbance increases without bound. In particular, when the initial perturbation is a spheroidal distortion, that is, when

$$f_2(0) = c, \quad f_n(0) = 0 \quad (n \neq 2),$$

the drop will develop an inward or outward spike depending on whether $c < 0$ or $c > 0$. In view of the fact that the former is consistent with the nature of drop deformation observed in our laboratory, we next investigate the consequences of this initial condition.

Figure 6 shows the evolution of the contour of an initially oblate spheroidal drop, as obtained by numerically integrating Eq. (7) using a fourth-order Runge–Kutta scheme and successively taking an increasing number of terms to account for the shift in the spectrum of the disturbance. It is seen that the distortion decays everywhere except in the vicinity of $\theta = 0$, where the perturbation grows. This behavior is identical to that given by Eqs. (10), and in turn both results are in qualitative agreement with the experimental findings which were summarized in the introduction, provided that the drop is assumed to be an oblate spheroid at $t = 0$.

We shall now extend the stability analysis to a drop with a small but nonzero interfacial tension. We first recall that, at $N = 0$, the "spectrum" of disturbances was seen to move away from the initially perturbed mode, and hence a similar behavior for f would be expected when $N > 0$. In particular, if only a finite number of f_n's is perturbed at $t = 0$, the number of terms which are significant at any instant of time will remain finite, however large. Moreover, since the conclusion reported earlier regarding the eigenvalues of the matrix A_M holds for any arbitrarily large value of M, we can conclude that the amplitude of the spectrum of disturbances will decay exponentially with time provided, of course, that the sum of the terms does not become so large within the time interval of $O(1/N)$ as to violate the assumption that the deviation from a spherical shape is small. In turn, this conclusion would seem to suggest that the effect of the interfacial tension should be vanishingly small at this level of approximation in order for the theory to be in agreement with the experiments. Unfortunately, one obvious shortcoming of this creeping flow analysis in the absence of interfacial tension is that the evolution of the drop boundary is completely determined by and is very sensitive to the assumed initial shape of the drop; for example, the numerically completed drop contour will generate the depression observed experimentally only if we specify that $g(\theta, t = 0) < 0$ near $\theta = 0$ whereas, in the experiments, the initial conditions were not carefully controlled. We shall show later on that the inclusion of inertial effects will partially resolve this deficiency of the theory.

In summary, the foregoing analysis, subject to the assumption of axisymmetry and the restriction that r defining the surface of the drop is single valued at each θ, has estab-

lished that, besides the sphere, there cannot exist a slightly deformed spherical drop shape on which the steady boundary conditions are satisfied exactly under creeping flow conditions. We have seen further that, if the interfacial tension is nonzero, the coefficient multiplying each harmonic in the expression for an initially slightly nonspherical drop shape consists of a sum of exponentially decaying functions of time. Finally, in the absence of interfacial tension, a numerical integration of Eq. (7) has shown that, when the initial configuration of the drop is assumed to be an oblate spheroid, the computed evolution of the drop shape is in qualitative agreement with the experimental observations and that the distortion on the drop boundary imposed at $t = 0$ gets swept to the rear by the external flow.

III. SLENDER TOROIDAL DROPS

In the preceding section, we traced the growth of small, axisymmetric distortions on a spherical drop as a step towards understanding the experimentally observed formation of an open fluid torus. We now turn our attention to the expansion of toroidal drops. A major mathematical difficulty which arises in developing the analysis is our lack of knowledge concerning the exact cross-sectional geometry of the drop. However, in the limit of a highly expanded drop, the problem becomes two-dimensional to first order near the drop surface, and by analogy to the three-dimensional case where the spherical shape was found to represent a feasible steady-state configuration, we may anticipate that, to leading order, the cross section of a very thin fluid ring will be circular and steady. This suggests that we examine a slender toroidal drop whose body centerline radius b is much larger than the "radius" ϵb of its cross section, where $\epsilon \ll 1$. Aside from circumventing the aforementioned mathematical difficulty, such an asymptotic approach also enables us to investigate the question of whether or not there exists a limiting cross-sectional geometry such that a drop possessing this cross section expands asymptotically without change of shape as $b \to \infty$.

As before, we assume that the flow is axisymmetric, that both fluids are incompressible and inertialess, and that the external fluid is unbounded at infinity. The analysis which follows is carried out for the case of a falling drop and can be readily modified for a rising drop.

It should be noted first of all that, in the absence of interfacial tension, the linearity of the resulting governing equations and the boundary conditions gives that if a drop with a certain specific configuration is found to expand, it must contract upon reversal of the external flow, or equivalently, of gravity. In particular, owing to the reversibility property of the solution of such systems, any drop whose body centerline radius changes with time cannot have a cross-sectional geometry which is symmetric about the plane $z = 0$ (cf. Fig. 7). Although we shall be concerned at first primarily with the case $N = 0$, the effects of a finite interfacial tension will be included in the analysis since we shall be examining the condition of nonzero N in a later section.

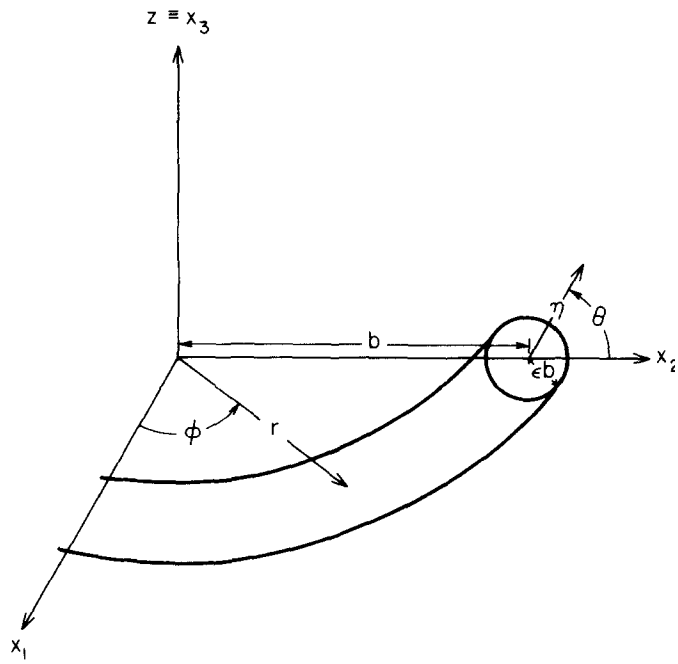

FIG. 7. Coordinate systems for the analysis pertaining to the motion of an open torus.

We shall develop the solution using the method of matched asymptotic expansions whereby the flow field is supposed to consist of two regions: the outer region of characteristic length scale b within which the problem reduces to that of a uniform flow past a line torus to leading order, and the inner region in the vicinity of the drop where the characteristic length scale is ϵb and, as a first approximation, the drop appears as a straight, circular cylinder. As before, the stream function will be expanded in powers of ϵ, where the order in ϵ will be designated by superscripts. In addition, the quantities in the inner region exterior to the drop will be distinguished from those in the outer region by a tilde.

A. First-order Stokes solution

We begin by seeking the leading-order solution in the outer region in terms of the cylindrical coordinates (r,ϕ, z) with the origin fixed at the center of the fluid torus as shown in Fig. 7. As mentioned above, the characteristic length scale far away from the drop is b; thus the nondimensionalization is carried out with respect to U, b, and $\mu U/b$, respectively, for the velocity, the length, and the stresses, and the stream function ψ satisfies

$$\left(\nabla^2 - \frac{2}{r}\frac{\partial}{\partial r}\right)^2 \psi = 0. \tag{11}$$

Following a standard procedure for slender bodies, we can readily carry out the analysis at this level of approximation by representing the flow field induced by the presence of the drop as due to a distribution of Stokeslet singularities along the body centerline $r = 1$, $z = 0$, with, in this case, a constant Stokeslet strength in the z direction. In other words, the velocity components are given, for a falling drop, by

$$u_z = 1 - \frac{F}{8\pi}\int_0^{2\pi} \frac{r^2 + 1 + 2z^2 - 2r\cos\phi}{(r^2 + 1 + z^2 - 2r\cos\phi)^{3/2}}\, d\phi, \tag{12a}$$

$$u_r = -\frac{F}{8\pi}\int_0^{2\pi} \frac{z(r - \cos\phi)}{(r^2 + 1 + z^2 - 2r\cos\phi)^{3/2}}\, d\phi, \tag{12b}$$

which satisfy the condition of uniform flow as $r^2 + z^2 \to \infty$. Performing the integration with respect to ϕ in Eqs. (12) yields

$$u_z = 1 - \frac{F}{8\pi}\left(\frac{2mK(m)}{r^{1/2}} + \frac{2z^2 mE(m)}{r^{1/2}[(r-1)^2 + z^2]}\right), \tag{13a}$$

$$u_r = -\frac{F}{8\pi}\left(\frac{zmK(m)}{r^{3/2}} + \frac{zmE(m)}{r^{3/2}}\frac{(r^2 - 1 - z^2)}{(r-1)^2 + z^2}\right), \tag{13b}$$

$$m = 2r^{1/2}[(r+1)^2 + z^2]^{-1/2},$$

where $K(m)$ and $E(m)$ are the complete elliptic integrals of the first and second kinds, respectively.

We next proceed with the inner expansion in order to satisfy the boundary conditions on the drop surface. Following Johnson and Wu,[8] we introduce the curvilinear orthogonal coordinate system (η_1, θ, ϕ) defined by

$$r = 1 + \eta_1 \cos\theta, \quad z = \eta_1 \sin\theta,$$

which transforms the outer coordinates to those of the inner expansion. In the neighborhood of the drop the flow field can be treated in two dimensions since the curvature of the drop can be neglected to this order of approximation. Thus the appropriate coordinate system consists of the two-dimensional cylindrical coordinates (η, θ) with the origin $\eta = 0$ coinciding with the center of the cross section of the drop (see Fig. 7), and the surface of the drop is approximated by $\eta = 1$. The characteristic length scale for η is ϵb so that $\epsilon\eta = \eta_1$. Also $\tilde{\psi}^{(0)}$ and $\hat{\psi}^{(0)}$ satisfy the biharmonic equation,

$$\nabla^4 \tilde{\psi}^{(0)} = 0, \quad \nabla^4 \hat{\psi}^{(0)} = 0,$$

and the steady-state boundary conditions at the drop interface. That the latter is exactly circular is an assumption which must be verified *a posteriori*, since the formulation of the problem becomes invalid if the steady boundary conditions fail to be satisfied to leading order at $\eta = 1$.

For the purpose of matching the two expansions, we must express Eqs. (13a) and (13b) in terms of the inner variables η and θ; to this end, we let $\epsilon \to 0$ with η fixed using the asymptotic forms of $K(m)$ and $E(m)$ as $m \to 1$, and recast the velocity components in terms of u_η and u_θ. This yields

$$u_\eta \to \sin\theta - (F/4\pi)(1 + \ln 8/\epsilon\eta)\sin\theta + (F/16\pi)\epsilon\eta \sin 2\theta + O(\epsilon^2), \tag{14a}$$

$$u_\theta \to \cos\theta - (F/4\pi)(\ln 8/\epsilon\eta)\cos\theta - (F/8\pi)\epsilon\eta(1 - \ln 8/\epsilon\eta) + O(\epsilon^2), \tag{14b}$$

so that, on solving for $\tilde{\psi}^{(0)}$ and $\hat{\psi}^{(0)}$ subject to the steady boundary conditions at $\eta = 1$ and matching the appropriate velocity components as $\eta \to \infty$ with the first two terms of Eqs. (14a) and (14b), we obtain[6]

$$\tilde{\psi}^{(0)} = [A_1^{(0)}(\eta^{-1} - \eta) + B_1^{(0)}\eta \ln\eta]\cos\theta,$$

$$\hat{\psi}^{(0)} = [\lambda^{-1} A_1^{(0)}(\eta^3 - \eta)]\cos\theta,$$

$$-B_1^{(0)} = -\frac{2(1+\lambda)}{\lambda} A_1^{(0)} = \frac{F}{4\pi} = \frac{1+\lambda}{(1+\lambda)\ln(8/\epsilon) + 1 + \lambda/2},$$

which, for $\lambda \to \infty$, reduces to the result of Johnson and Wu[8] contained in their Eq. (23) for a uniform flow past a rigid torus. Since the matching requirement as well as the steady boundary conditions on the surface of the drop have been satisfied exactly, if follows that, to first order, the cross-sectional geometry of the drop can be given by a circle and that time dependence appears only implicitly via $\epsilon(t)$.

B. Curvature effects

We now include the effect of curvature in the inner expansion and proceed to $O(\epsilon)$. To begin with, the requirement that the volume of the drop be conserved yields

$$\frac{db}{dt} + \frac{2}{3} b \frac{d\epsilon}{dt} = 0,$$

which, together with the fact that $b^{-1} = O(\epsilon^{2/3})$ implies that the rate of change of the radius of the cross section is $O(\epsilon^{2/3})$ smaller than that of b and hence will not enter into our analysis to this order. We also observe that, since the total drag exerted on the drop is always balanced by the downward force due to gravity and is constant, the product $U(t)b(t)B_1^{(0)}(t)$ is independent of time. Lastly, the equation for the cross-sectional radius of the drop is written as

$$R(\theta, t) = 1 + \epsilon(t)\sum_{n=2}^{\infty}[T_n(t)\cos n\theta + S_n(t)\sin n\theta] + O(\epsilon^2),$$

where the terms with $n = 0$ and $n = 1$ have been omitted in order that the volume of the drop may be conserved and that the origin remain fixed at the center of mass of the cross section.

The flow is no longer two-dimensional nor axisymmetric in the inner region owing to the effect of the curvature of the body centerline; thus at this order, the full curvilinear coordinate system (η, θ, ϕ) must be retained. In particular, expanding the equation of continuity to $O(\epsilon)$ gives

$$\frac{\partial}{\partial\eta}[\eta(u_\eta^{(1)} + \eta u_\eta^{(0)}\cos\theta)] + \frac{\partial}{\partial\theta}(u_\theta^{(1)} + \eta u_\theta^{(0)}\cos\theta) = 0,$$

and hence by setting

$$u_\eta^{(1)} = u_\eta'^{(1)} - \eta u_\eta^{(0)}\cos\theta, \tag{15a}$$

$$u_\theta^{(1)} = u_\theta'^{(1)} - \eta u_\theta^{(0)}\cos\theta, \tag{15b}$$

we can define the stream functions $\tilde{\psi}^{(1)}$ and $\hat{\psi}^{(1)}$ corresponding to $\tilde{\mathbf{u}}'$ and $\hat{\mathbf{u}}'$, respectively, since $\mathbf{u}'$ is then divergence-free in the coordinates η and θ.

The equations governing $\tilde{\psi}^{(1)}$ and $\hat{\psi}^{(1)}$ are derived by expanding the creeping flow equations of motion in powers of ϵ and become[6]

$$\nabla^4 \hat{\psi}^{(1)} = -4B_1^{(0)}\eta^{-2}\cos 2\theta, \quad \nabla^4 \hat{\psi}^{(1)} = 16A_1^{(0)}/\lambda.$$

In accordance with Eqs. (15), $-\eta \mathbf{u}^{(0)}\cos\theta$ must be added to the velocity components associated with the above stream functions, and the combined expressions in turn are subject to the boundary conditions at $\eta = R(t, \theta)$, with (3) replaced by

$$\tilde{\mathbf{u}} \cdot \mathbf{n} = \hat{\mathbf{u}} \cdot \mathbf{n} = \frac{\epsilon b}{U} \frac{\partial R/\partial t^*}{|\mathbf{i}_\eta - \nabla R|} + \frac{1}{U}\frac{db}{dt^*}\cos\theta, \tag{3'}$$

where $\mathbf{i}_\eta$ is a unit vector in the η direction, in order to account for the radial motion of the body centerline. When in addition the matching requirement as $\eta \to \infty$ is satisfied, the following set of coupled differential equations involving S_n, T_n, and b is obtained[6]:

$$\frac{d\tilde{b}}{dt} = -\frac{1}{8}\tilde{b}^{-5/2}\frac{3+\lambda^2}{(1+\lambda)^2}S_2 - \tilde{b}^{-3/2}N_c\frac{1}{8(1+\lambda)} \times\left[4 + 2\ln\frac{8}{\epsilon} + \lambda\left(3 + 2\ln\frac{8}{\epsilon}\right)\right], \tag{16a}$$

$$\frac{dS_n}{dt} = -\frac{1}{2}nN_c\tilde{b}^{1/2}S_n + \frac{\tilde{b}^{-1/2}}{8(1+\lambda)(n^2-1)} \times\left((n^3-3n-2)T_{n-1} + (n^3+n-2)T_{n+1} + \frac{3+8\lambda}{2(1+\lambda)}\delta_{n2}\right), \tag{16b}$$

$$\frac{dT_n}{dt} = -\frac{1}{2}nN_c\tilde{b}^{1/2}T_n + \frac{\tilde{b}^{-1/2}}{8(1+\lambda)(n^2-1)} \times[(-n^3+3n+2)S_{n-1} + (-n^3-n+2)S_{n+1}].$$

In the above, the nondimensionalization used previously has been modified such that the characteristic length is given by

$$l = (V/2\pi^2)^{1/3}, \quad V = 2\pi^2 b^3\epsilon^2,$$

the characteristic velocity by

$$U_c = l^2 g\Delta\rho/\mu,$$

the characteristic time by

$$l/U_c = \mu/lg\Delta\rho,$$

and the new inverse capillary number by

$$N_c = \gamma/l^2 g\Delta\rho,$$

where $\Delta\rho$ refers to the difference in the density of the drop and that of the ambient fluid; in particular, we have $\tilde{b} = b(t)/l$.

Equation (16a) gives the rate of change of the body centerline radius, and the expression on the right-hand side consists of two terms: the first is proportional to S_2 and is positive if and only if $S_2 < 0$, whereas the second term arises from the presence of the interfacial tension and is always negative. In turn, the evolution of S_2 with time is governed by Eqs. (16b) and (16c) and is seen to be determined by even S_n's and odd T_n's. Note, however, that there is an inhomogeneous term at $n = 2$ in Eq. (16b) which arises from the effect of the body centerline curvature and which tends to render S_2 more positive. That this effect causes the drop cross section to stretch along the 45° axis can also be anticipated from the limiting form of $\tilde{\mathbf{u}}^{(1)}$ as $\eta \to \infty$ [see Eq. (14a)] whose η component has the maximum rate of extension along the axis $\theta = 45°$ and that of compression at $\theta = 135°$.

It is evident that the necessary condition for a toroidal drop to expand at this order is given by $S_2 < 0$; that is, the drop cross section must be elongated along the 135° axis for it to drift away from the center of mass in a manner similar to the oblique fall in the gravitational field of a body having an elliptical cross section. Moreover, since the interfacial tension serves only to impede the expansion of the ring, we first assume that the interfacial tension is negligibly small, and investigate in detail the functional dependence of S_2 on time by setting $N_c = 0$. In this case, we again find it illuminating to examine Eqs. (16b) and (16c) in the asymptotic limit as $n \to \infty$ which become, respectively,

$$8(1+\lambda)\tilde{b}^{1/2}\frac{dS_n}{dt} = \left(n(T_{n-1}+T_{n+1}) + \frac{1}{6}\frac{3+8\lambda}{1+\lambda}\delta_{n2}\right) \times\left[1 + O\left(\frac{1}{n^2}\right)\right], \tag{17a}$$

and

$$8(1+\lambda)\tilde{b}^{1/2}\frac{dT_n}{dt} = -n(S_{n-1}+S_{n+1})\left[1 + O\left(\frac{1}{n^2}\right)\right]. \tag{17b}$$

Denoting

$$h \equiv \sum_{n=1}^{\infty} T_n\cos n\theta + S_n\sin n\theta,$$

we can easily show that, on neglecting the $O(1/n^2)$ terms, Eqs. (17) become identical to

$$\frac{\partial h}{\partial \tau} + \cos\theta\frac{\partial h}{\partial\theta} = h\sin\theta + \frac{1}{12}\frac{3+8\lambda}{1+\lambda}\sin 2\theta, \tag{18}$$

$$\frac{d\tau}{dt} = [4(1+\lambda)\tilde{b}^{1/2}]^{-1}.$$

As before, although the requirement that both $S_1(t)$ and $T_1(t)$ remain zero is not satisfied, Eq. (18) nevertheless yields solutions which describe qualitatively the evolution of the drop contour. On solving Eq. (18) using the method of characteristics, we obtain that

$$h(\tau) = h(0)\frac{2\exp(\tau)}{(1-\sin\theta)\exp(2\tau) + 1 + \sin\theta} + \frac{\frac{1}{3}[(3+8\lambda)/(1+\lambda)]\cos\theta\exp(2\tau)}{[(1-\sin\theta)\exp(2\tau) + 1 + \sin\theta]^2} - \frac{1}{12}\frac{3+8\lambda}{1+\lambda}\cos\theta, \tag{19a}$$

along the characteristics

$$\frac{1+\sin\theta}{1-\sin\theta}\exp(-2\tau) = \frac{1+\sin\theta(0)}{1-\sin\theta(0)}. \tag{19b}$$

Evidently, in the limit as $\tau \to \infty$, the first two terms on the right-hand side of Eq. (19a) decay exponentially everywhere

except in the region

$$|\theta - \tfrac{1}{2}\pi| \leqslant \exp(-\tau),$$

where they become proportional to $h(0)\exp(\tau)$ and $(\frac{1}{2}\pi - \theta)\exp(2\tau)$, respectively. This behavior accurately models the solution of Eqs. (16b) and (16c) which, when integrated numerically using series truncation and a fourth-order Runge–Kutta method, with t replaced by τ, $\lambda = 4$, $N_c = 0$, and with initial conditions $S_n(0) = T_n(0) = 0$, yielded a steady drop shape as $\tau \to \infty$ except in a small region near $\theta = \frac{1}{2}\pi$, where the drop was found to develop sharp peaks that grew steadily in time.

In view of the fact that, according to both the numerical and the approximate solution of Eqs. (16a) and (16c), h approaches a steady state except near the rear stagnation point $\theta = \frac{1}{2}\pi$, we shall seek the asymptotic value of S_2 as $\tau \to \infty$ by considering the steady-state form of Eq. (18). We recall, however, that according to this equation, $T_1(\tau)$ does not remain zero and moreover appears in the expression governing S_2, as seen from Eqs. (17a) and (17b):

$$\frac{dT_1}{d\tau} = -\frac{1}{2}S_2, \quad \frac{dS_2}{d\tau} = \frac{1}{2}(T_1 + T_3) + \frac{1}{12}\frac{3+8\lambda}{1+\lambda}.$$

But since, as mentioned earlier, only odd T_n's and even S_n's determine S_2, we can eliminate this error by merely adding the term $\frac{1}{2}S_2\cos\theta$ to the right-hand side of Eq. (18) thereby obtaining

$$\frac{\partial h}{\partial \tau} + \frac{\partial}{\partial \theta}h\cos\theta = \frac{1}{12}\frac{3+8\lambda}{1+\lambda}\sin 2\theta + \frac{1}{2}S_2\cos\theta, \tag{18'}$$

which now satisfies the condition

$$\frac{dT_1}{d\tau} = 0.$$

Hence T_1 can be set equal to zero in the differential equation for S_2 given above. Moreover, by requiring that h remain finite at $\theta = -\pi/2$, we find from Eq. (18′) that, at steady state,

$$h\cos\theta = -\frac{1}{24}\frac{3+8\lambda}{1+\lambda}\cos 2\theta + \frac{1}{2}S_2\sin\theta + \frac{1}{2}\left(S_2 - \frac{1}{12}\frac{3+8\lambda}{1+\lambda}\right),$$

which also satisfies the consistency check $S_2 = S_2$ when multiplied through by $\sin\theta$ and integrated from $\theta = 0$ to $\theta = 2\pi$. Furthermore,

$$\frac{1}{\pi}\int_0^{2\pi}\cos\theta h\, d\theta \equiv T_1 \equiv 0 = S_2 - \frac{1}{12}\frac{3+8\lambda}{1+\lambda},$$

which gives $S_2 = \frac{1}{12}(3+8\lambda)/(1+\lambda)$. Numerical integrations of Eqs. (16b) and (16c) with $\lambda = 4$ and $N_c = 0$ for the three initial conditions $S_2(0) = -1$, $S_2(0) = 0 < \frac{1}{12}(3+8\lambda)/(1+\lambda)$, and $S_2(0) = 1 > \frac{1}{12}(3+8\lambda)/(1+\lambda)$ indeed showed that, in time, S_2 approached the same constant value given by $1.102 \times [\frac{1}{12}(3+8\lambda)/(1+\lambda)]$. In other words, even if we choose $S_2(0) < 0$ and have an expanding drop for a finite time interval, the toroidal drop will eventually begin to contract even in the absence of interfacial tension if inertial effects are assumed negligible. Moreover, it follows immediately from Eqs. (16) that if N_c is nonzero, the interfacial tension deters the growth of surface disturbances, and in addition enhances the tendency of the drop to contract.

It is evident therefore that a creeping flow analysis cannot explain the experimentally observed expansions of toroidal drops, and that the influence of small but finite inertia must be included in the theory. It should also be noted that there is an inconsistency in the zero Reynolds number assumption in the limit as $\epsilon \to 0$ because, on equating the buoyancy force to the drag, we obtain

$$\frac{8\pi^2 b\mu U(1+\lambda)}{(1+\lambda)\ln(8/\epsilon) + 1 + \lambda/2} = V\Delta\rho g,$$

from which it follows that

$$R_b = \frac{\rho b U}{\mu} = \frac{V(\Delta\rho)g}{8\pi^2\mu^2}\frac{(1+\lambda)\ln(8/\epsilon) + 1 + \lambda/2}{1+\lambda}.$$

Hence R_b grows logarithmically as $\epsilon \to 0$ and the validity of the creeping flow assumption becomes questionable in this limit. Of course, since we are not necessarily interested in vanishingly small values of ϵ but rather in understanding our experimental findings where ϵ was only moderately small, we could always confine our study to the case $R_b \ll 1$ by choosing $\Delta\rho V/\mu^2$ to be arbitrarily small. Nonetheless, in light of the failure of the above analysis to provide an explanation for experiments, we shall next investigate the effect of small but nonzero inertia on the drop deformation.

IV. INERTIAL EFFECTS

A. Spherical drops

We first turn our attention to the deformatin of spherical drops in the presence of inertia. Taylor and Acrivos[4] obtained steady solutions for the case in which the Reynolds number $\mathrm{Re} \equiv \rho a U/\mu$ was assumed to be small but nonzero by the method of singular perturbation expansions and showed that the drop cannot remain spherical [see their Eq. (21)]. In fact, only a slight modification of their results is needed to trace the deformation of a spherical or a nearly spherical drop, and the evaluation of appropriate time-dependent boundary conditions at the drop interface yields an inhomogeneous term at $n = 2$ in Eq. (4) which now becomes

$$G_n\frac{a}{U}\frac{df_n}{dt^*} = -H_n f_{n+1} - Q_n f_n + W_n f_{n-1} - \delta_{n2}\alpha_0, \tag{20}$$

$$\alpha_0 = \frac{200 + 638\lambda + 684\lambda^2 + 243\lambda^3}{48(1+\lambda)} - \frac{5}{12}\kappa,$$

where κ is the density ratio, $\kappa = \hat{\rho}/\rho$. In deriving Eq. (20), we have assumed, for the sake of simplicity, that the drop is initially exactly spherical, and have consequently replaced the small parameter δ introduced in Sec. II B by Re. Although the sign of the inhomogeneous term depends on the value of κ, it has been pointed out by Taylor and Acrivos that in all cases of physical interest α_0 is positive.

If γ is set equal to zero, we can extend the asymptotic analysis of Eq. (4) as $n \to \infty$ by adding an inhomogeneous

term to the right-hand side of Eq. (9) so that

$$\frac{\partial f}{\partial t} - \frac{1}{2(1+\lambda)} \sin\theta \frac{\partial f}{\partial \theta} = \frac{\cos\theta}{1+\lambda} f - \alpha_1 P_2, \quad \alpha_1 \equiv \frac{5\alpha_0}{G_2}, \tag{21}$$

which has the solution

$$f(t) = (1+\lambda)\alpha_1 \cos\theta + [f(0) - (1+\lambda)\alpha_1 \cos\theta(0)] \times \left(\frac{1+\cot^2\theta/2}{1+\cot^2\theta(0)/2}\right)^2 \exp\left(\frac{-t}{1+\lambda}\right), \tag{22}$$

along the characteristics given by Eq. (10b). Expanding Eq. (22) at small time yields

$$f = f(0) - t\{\alpha_1 P_2 - [f(0)/(1+\lambda)]\cos\theta\} + o(t),$$

while, as $t \to \infty$,

$$f \to [f(0) - (1+\lambda)\alpha_1]\exp(t/1+\lambda),$$

at $\theta = 0$ and

$$f \to [f(0) + (1+\lambda)\alpha_1]\exp(-t/1+\lambda),$$

at $\theta = \pi$.

Clearly, then, the effect of inertia is to render the drop more like an oblate spheroid, thereby favoring the formation of the depression at the rear stagnation point. The same tendency, although not as pronounced, also exists even in the presence of small interfacial tension owing to the term $-\alpha_0 \delta_{n2}$ in the governing equation (20). On the other hand, the asymptotic expression for f at $\theta = 0$ in the limit of large t suggests that if the drop resembles a prolate spheroid whose eccentricity is such that $f(0) > (1+\lambda)\alpha_1$ near the rear stagnation point, the depression will not form. Indeed, a numerical integration of Eq. (20) with $\lambda = 4$, $\kappa = 2$, $N = 0$, and initial conditions $f_2(0) = 1 \simeq 3(1+\lambda)\alpha_1, f_n(0) = 0\ (n \neq 2)$, using series truncation and a fourth-order Runge–Kutta scheme confirmed that the protrusion near the rear stagnation point grows with time and that a depression is not formed. Hence our analysis has not completely eliminated the dependence of the drop deformation on its initial configuration, if the latter deviates only slightly from the spherical shape.

B. Slender toroidal drops

When, in addition to curvature, inertial effects are considered in the case of slender toroidal drops, the development presented in Sec. III gives rise to a double expansion in the parameters R_b and ϵ, where $R_b \equiv \rho b U/\mu$. We shall assume $R_b \ll 1$ and shall seek the leading-order Reynolds number correction to the rate of drop expansion by examining the flow field which now consists of three regions exterior to the drop: (1) the Oseen region where the length scale is $\mu/\rho U$ and inertial effects must be retained even to first order, (2) the Stokes outer region where the length scale is b and inertial terms based on R_b are negligible to leading order, and finally (3) the Stokes inner region where the length scale is ϵb and ϵR_b is set equal to zero to the present level of approximation.

The analysis in the Oseen region where $R_b|\mathbf{x}| \sim O(1)$ is readily available in many standard references (cf. Ref. 9) since, to the present order of interest, the first two terms of the stream function Ψ are identical to those for the problem of flow past a point force along the z axis the magnitude of which has already been obtained by the creeping flow analysis. When Ψ is expressed in Stokes outer variables and expanded for small R_b for the purpose of matching, it reduces to

$$\Psi = -\frac{1}{2} r^2 + \frac{F r^2}{4(r^2+z^2)^{1/2}} - \frac{1}{16} F R_b r^2 \left(1 - \frac{z}{(r^2+z^2)^{1/2}}\right) + \ldots, \tag{23}$$

as $R_b \to 0$. The matching as well as the rest of the analysis is simplified if we define the integral

$$J = \int_0^{2\pi} (r^2 + 1 + z^2 - 2r\cos\phi)^{1/2}\, d\phi,$$

in terms of which the Stokes outer stream function, corresponding to Eqs. (13), can be expressed as

$$\psi = \frac{F}{8\pi} r \frac{\partial J}{\partial r} - \frac{1}{2} r^2,$$

which matches the first two terms in Eq. (23) as $r^2 + z^2 \to \infty$. From the form of Eq. (23), it is apparent that the leading-order inertial correction term in the Stokes outer expansion is of $O(R_b)$, and thus for our purposes, we seek particular solutions to the Navier–Stokes equations of motion written as

$$-\frac{\partial P}{\partial x_i} + \nabla^2 u_i = R_b \left(\delta_{j3} \frac{\partial u_i}{\partial x_j} + (u_j - \delta_{j3}) \frac{\partial u_i}{\partial x_j}\right), \tag{24}$$

where δ_{j3} is a unit vector in the $+z$ direction, and where u_i on the right-hand side is given by the expressions in Eqs. (13).

The particular integral corresponding to the first term on the right-hand side of Eq. (24) can be obtained analytically and the corresponding expression for the stream function is given by

$$R_b \frac{F}{32\pi} rz \frac{\partial J}{\partial r}, \tag{25}$$

which, incidentally, matches with the term $\frac{1}{16} F R_b r^2 z (r^2+z^2)^{-1/2}$ of Eq. (23) as $r^2 + z^2 \to \infty$. The other term $-\frac{1}{16} F R_b r^2$ in Eq. (23) is matched by a multiple of the Stokes solution. When the velocity components derived from Eq. (25) are expressed in Stokes inner variables and evaluated near the drop by letting $r \to 1$ and $z \to 0$, we find, to first order, that the resulting velocity makes a nonzero contribution to u_r given by

$$\frac{R_b}{8\pi} F \equiv \frac{1}{2} \frac{1+\lambda}{(1+\lambda)\ln(8/\epsilon) + 1 + \lambda/2} R_b, \tag{26}$$

while the correction to u_z vanishes identically at $O(R_b)$. In other words, in the matching region, the above contributes a uniform radial flow in the outward direction.

An alternative derivation of Eq. (26) is to distribute Oseenlets of constant strength F on the body centerline of the ring with their direction along the positive z axis.[6] We evaluate the contribution of each Oseenlet to the flow field at $z = 0$ and rewrite the resulting expressions in terms of Stokes outer coordinates by taking the limit $R_b \to 0$ while holding r fixed. Because of axisymmetry, u_1 is equivalent to u_r at $\phi = 0$ in the

present problem; in particular, the Oseenlet placed at $\phi = \phi_0$ gives rise to a value for u_1, evaluated at $\phi = 0$,

$$(F/32\pi)\cos[(\pi - \phi_0)/2]\, R_b,$$

which, when integrated along the ring, leads to Eq. (26). Note that, according to this alternative derivation, Eq. (26) is valid when $R_b = O(1)$, and only requires that $\epsilon R_b \ll 1$. A positive value for the inertial correction to u_r is consistent with the fact that the Oseenlets generate within the wake directly behind the drop an inflow towards the drop which must be compensated by an outward radial flow to assure that the net volume flux through any surface enclosing the body be zero.

A particular solution corresponding to the remaining inhomogeneous term in Eq. (24), if written in a closed form, involves a volume integral obtained by means of Green's functions techniques. Following Happel and Brenner[10] (pp. 79–81), we find

$$u_i'(\mathbf{x}^0) = -\frac{R_b}{8\pi}\int_V V_{ik}(\mathbf{x}-\mathbf{x}^0)[u_j(\mathbf{x}) - \delta_{j3}]\frac{\partial u_k(\mathbf{x})}{\partial x_j}\, dV_x, \tag{27}$$

$$V_{ik}(\mathbf{y}) = \frac{\delta_{ik}}{|\mathbf{y}|} + \frac{y_i y_k}{|\mathbf{y}|^3}, \quad \mathbf{y} = \mathbf{x} - \mathbf{x}^0,$$

where $\mathbf{u}'$ is the velocity arising from the second inhomogeneous term in Eq. (24), $\mathbf{u}$ within this integral is given by Eqs. (13), $\mathbf{x}^0$ is any specified point outside the drop at which we seek a solution, and the integration is performed over the entire volume external to the drop. Since $u_i - \delta_{i3}$ decays as $|\mathbf{x}^0|^{-1}$ away from the drop, the integral in Eq. (27) is clearly bounded. As before, we set $i = 1$ in Eq. (27) and simplify the integral by choosing $\mathbf{x}^0$ to fall on the body centerline such that $x_1^0 = 1$, $x_2^0 = 0$, and $x_3^0 = 0$. The integration with respect to ϕ can be readily carried out, but that with respect to r and z must be performed using analytical as well as numerical techniques. The computation is tedious but fairly straightforward[6] and finally yields $u_1' = 1.73(B_1^{(0)})^2 R_b$.

Having obtained the first-order inertial correction to the creeping flow solution, we turn our attention to the Stokes inner expansion. To the present level of approximation, we have $\epsilon = 0$, and hence we need only to modify the leading term $\tilde{\psi}^{(0)}$. Matching requires that

$$\tilde{\psi}^{(0)} = [A_1^{(0)}(-\eta + \eta^{-1}) + B_1^{(0)}\eta \ln \eta]\cos\theta + R_b[-\tfrac{1}{2}B_1^{(0)} + 1.73(B_1^{(0)})^2]\eta \sin\theta, \tag{28a}$$

$$\hat{\psi}^{(0)} = \lambda^{-1}A_1^{(0)}(\eta^3 - \eta)\cos\theta + R_b[-\tfrac{1}{2}B_1^{(0)} + 1.73(B_1^{(0)})^2]\eta \sin\theta, \tag{28b}$$

and Eq. (16a) is replaced by

$$\frac{d\tilde{b}}{dt} = \frac{\rho g \Delta\rho l^3}{16\mu^2}\left(-\frac{1}{2B_1^{(0)}} + 1.73\right)\tilde{b}^{-1} - \frac{1}{8}\tilde{b}^{-5/2}\frac{3+\lambda^2}{(1+\lambda)^2}S_2 - \tilde{b}^{-3/2}N_c\frac{1}{8(1+\lambda)} \times\left[4 + 2\ln\frac{8}{\epsilon} + \lambda\left(3 + 2\ln\frac{8}{\epsilon}\right)\right]. \tag{29}$$

Note that, in contrast to the case of a nearly spherical drop where inertia was seen to play a dominant role in determining the first-order deformation, here inertia does not affect the cross-sectional geometry and, more specifically, S_2, which enters into the expression for the rate of change of the drop body centerline radius. This is because inertia gives rise to a constant outward radial flow in the neighborhood of the drop causing it to expand irrespective of its cross-sectional shape even if the assumption that the latter is nearly circular is removed.

If $\epsilon \ll R_b \ll 1$ so that the first term on the right-hand side of Eq. (29) is dominant, the rate of change of b depends, aside from the physical properties of the fluid, solely on $B_1^{(0)} \equiv -F/4\pi = -(1+\lambda)/[(1+\lambda)\ln(8/\epsilon) + 1 + \lambda/2]$. Integrating Eq. (29) keeping only the first term yields

$$\int_0^{\tilde{b}} \frac{dx^2}{\ln x^2 + c_1} = \frac{3}{64}\frac{\rho g(\Delta\rho) l^3}{\mu^2}\, t + \text{const},$$
$$c_1 = 7.4 + 2(2+\lambda)/3(1+\lambda). \tag{30}$$

It should be noted that according to Eq. (30), plots of $\tilde{b}$ vs $\rho(\Delta\rho)l^3 t/\mu^2$ for drops with different physical properties should collapse on a single curve when $\epsilon \ll R_b$. In fact, Eq. (30) should provide a good approximation for the rate of expansion regardless of the drop cross-sectional shape since under creeping flow conditions the drag on an object is in general quite insensitive to its geometry; hence we would not expect the expression for $B_1^{(0)}$ to differ substantially from that used above even if the drop cross section is noncircular.

On the other hand, if $\epsilon \equiv \tilde{b}^{-3/2}$ and R_b are comparable in magnitude, as is the case in our experiments, the three terms in Eq. (29) must be considered together. In particular, if the interfacial tension is negligible, the asymptotic value of S_2 should be used in the second term.

The foregoing theoretical investigation has identified the mechanism for the experimentally observed drop expansion as being due to inertial effects. We have shown that a slender fluid ring with any arbitrary cross-sectional geometry expands in the presence of inertia to first order in Reynolds number, and that the functional dependence of b on t at this level of approximation is given by Eq. (29). We have also shown that the effects of both curvature and of interfacial tension are to retard drop expansion. In what follows, we shall present experimental data to assess the merits of this theoretical analysis.

V. EXPERIMENTS

A. Materials and procedure

In order to test the theoretical development described above, a series of experiments was performed in our laboratory in which the rates of expansion of toroidal drops were measured using a cine camera. The fluid comprising both the drop and the bulk was Karo light corn syrup diluted with various proportions of water (see Table II for their physical properties) such that the density difference and the viscosity ratio fell in the range $0.031\ \text{g/cm}^3 \leqslant \Delta\rho \leqslant 0.071\ \text{g/cm}^3$ and $2.8 \leqslant \lambda \leqslant 11.6$, respectively. For the purpose of inhibiting bacterial growth, sodium azide and ethylene-diaminetetraacetic

TABLE II. The physical properties of the six systems used in the experiment.

	External fluid ρ (g/cm^3)	μ poises	Internal fluid $\Delta\rho$ (g/cm^3)	λ	Ambient temperature (°C)
System 1	1.264	0.51	0.071	11.6	14
System 2	1.264	0.51	0.065	7.7	14
System 3	1.274	0.61	0.057	7.1	21
System 4	1.274	0.61	0.040	4.0	21
System 5	1.287	0.77	0.041	3.9	24
System 6	1.287	0.77	0.031	2.8	24

acid (EDTA) were added to each mixture so that the final composition was approximately 0.2% by weight sodium azide and 6% molar EDTA. Since the temperature of the experiments varied from system to system, the fluid viscosities and densities were measured immediately after each run. The ambient fluid was contained in a plexiglass tank of square cross section (22.7×22.7 cm) and height 91.4 cm, and the liquid depth was 82 cm.

The drops were colored using red vegetable dye to provide the necessary contrast. In order to facilitate the formation of the ring, each drop was allowed to fall from a distance of approximately 5 cm above the free surface at the center of the tank, since this had the effect of flattening the drop. Unfortunately, under the experimental conditions presented in this section, each drop left a thin tail emanating from the rear stagnation point and this resulting loss of fluid eliminated the possibility of determining the volume of each drop by measuring its original weight. But since the best visual estimation from an enlargement of the film indicated that it was reasonable to approximate the drop cross section by a circle, a first estimate of the volume was obtained by measuring the thickness of the ring, correspnding to $2\epsilon b$, and its outer diameter, equivalent to $2b(1+\epsilon)$. These measurements were taken by placing a ruler at the center of the tank and using the film of the ruler as a calibration for the distances in each run. As a check, the settling speed of the ring was calculated using the value of the volume as obtained above by employing an expression for the drag which includes the leading-order Reynolds number correction[11]:

$$D/D_0 = 1 + (D_0/16\pi\mu bU)R_b,$$

where D is the actual drag on the body and D_0 is that given by the creeping flow analysis, $D_0 = 8\pi^2 b\mu U(1+\lambda)/[(1+\lambda)\ln(8/\epsilon) + 1 + \lambda/2]$. Because of its small magnitude and because the boundary between the drop and the surrounding fluid could not be easily distinguished on the film, the thickness of the ring was much more difficult to determine than the drop outer diameter, and hence the value of $2\epsilon b$ was adjusted, with $2b(1+\epsilon)$ kept fixed at its measured value, until this computed speed was within 10% of the measured speed. This took into consideration the fact that the theory for the drag applies only for a domain of infinite extent and in the limit as $\epsilon \to 0$, and consequently it overestimates the settling speed of the drop by approximately 10% for our experimental conditions. We therefore allowed the computed and the measured speeds to differ in order to account for the side wall effects[12] and for the errors arising from using the asymptotic form for D. In all the cases discussed below, the two volumes thus obtained were within 20% of each other, the averaged difference being 10%.

We mention parenthetically that at Reynolds numbers somewhat larger than those reported here, a drop hitting the free surface developed a depression at the rear stagnation point immediately upon entering the bulk medium without forming a tail. However, in view of the fact that our analysis was carried out under the assumption of small inertial effects and since comparisons with the theory would be difficult if the experiments were conducted for Reynolds numbers larger than unity, such systems were not investigated further.

The transient expansions were recorded using a cine camera (Bolex) with the optical axis perpendicular to the axis of symmetry of the ring, and the drop motion was filmed from the time ϵ was about $\frac{1}{2}$ to the onset of instability. The Reynolds numbers were in the range $0.15 \leqslant R_b \leqslant 0.7$, and for half the cases that were examined, $\epsilon > R_b$. During filming, the drops were no closer than 30 cm from the bottom of the tank, and hence the wall effects could be assumed to be very small.[12] Finally, the rate of change of b was obtained from the frame speed and the measurement of b.

B. Results

Six to eight data points were taken in each run, and representative data points from eight different runs are tabulated in Table III. The measured speeds are given in the first column, the values of b and ϵ obtained in the manner described in the preceding subsection are shown in the second and third columns, respectively, the computed speeds and the corresponding Reynolds numbers are given in the fourth and fifth columns, respectively, and the time-averaged measured rate of expansion is indicated in the sixth column.

The last three columns represent the three terms resulting from the effects of inertia, drop curvature, and the transient interfacial tension, respectively, which appear in the expression for the theoretically predicted rate of change of b, calculated from an alternative form of Eq. (29):

$$\frac{db}{dt^*} = UR_b\left(\frac{1}{2}|B_1^{(0)}| + 1.73|B_1^{(0)}|^2\right) - \epsilon U|B_1^{(0)}|\frac{3+\lambda^2}{2(1+\lambda)^2}S_2 - \epsilon\frac{\gamma}{\mu}\frac{1}{8(1+\lambda)}\left[4 + 2\ln\frac{8}{\epsilon} + \lambda\left(3 + 2\ln\frac{8}{\epsilon}\right)\right]. \tag{29'}$$

It is evident from the tables that if only the first term on the right-hand side of Eq. (29′) is retained, the rate of expansion is overestimated nearly by an order of magnitude. Of course, some disagreement is to be expected if the experimental measurements are compared to the theoretical predictions arising from the inertial contribution alone, since none of the above systems satisfy the condition $\epsilon \ll R_b$. However, it is important to note that the minimum discrepancy is found not in the system for which ϵ/R_b is the small-

TABLE III. Experimentally measured rates of expansion and the corresponding theoretical predictions.

System	Measured speed (cm/sec) ± 5%	b (cm) ± 10%	ϵ ± 15%	Computed speed (cm/sec) ± 10%	R_b ± 20%	db/dt^* (cm/sec) ± 30%	Inertia (cm/sec)	Curvature (cm/sec)	Interfacial tension (cm/sec)[a]
1	0.93	0.27	0.37	0.95	0.65	0.018	0.17	$-0.042\,S_2$	$-0.84\,\gamma$
2	0.90	0.26	0.42	1.00	0.65	0.015	0.19	$-0.050\,S_2$	$-0.93\,\gamma$
3[b]	0.95	0.31	0.41	1.02	0.66	0.017	0.19	$-0.049\,S_2$	$-0.76\,\gamma$
3[b]	0.75	0.28	0.39	0.81	0.47	0.011	0.11	$-0.036\,S_2$	$-0.73\,\gamma$
4[c]	0.82	0.31	0.44	0.88	0.57	0.013	0.14	$-0.042\,S_2$	$-0.81\,\gamma$
4[c]	0.42	0.19	0.49	0.47	0.19	0.005	0.026	$-0.026\,S_2$	$-0.88\,\gamma$
5	0.36	0.27	0.35	0.41	0.19	0.004	0.019	$-0.015\,S_2$	$-0.54\,\gamma$
6	0.32	0.25	0.40	0.34	0.14	0.003	0.013	$-0.014\,S_2$	$-0.60\,\gamma$

[a] γ has units mN/m.
[b, c] Drop sizes were varied.

est, but in system 6 which has the largest ϵ to R_b ratio. Clearly, the $O(\epsilon)$ terms must be retained in the theory and hence we shall next examine the effect of the curvature of the ring which impedes the expansion of the drop when $S_2 > 0$. It was shown in Sec. III B that, if the interfacial tension is assumed to be negligible, S_2 approaches in time a positive constant which lies within the range 0.275 ($\lambda = 0$) to 0.735 ($\lambda = \infty$). Although assigning these asymptotic values to S_2 in Eq. (29′) reduces the differences between the measured and the theoretical rates of expansion, significant discrepancies still remain which cannot be attributed solely to experimental error or to the asymptotic nature of the analysis. Moreover, if S_2 were as large as $\frac{1}{2}$, then since ϵ varied from 0.3 to 0.6, the magnitude of ϵS_2 would have been in the range of 0.13–0.3 which should have led to an observable surface distortion. As mentioned previously, however, a careful examination of the film appeared to indicate that the drop cross section possessed fore-and-aft symmetry, and no deviation from a circular cross section could be detected.

In light of the above findings, we shall examine therefore the possibility that a finite interfacial tension existed in all the systems which had a measurable effect on the rate of drop expansion.

C. Transient interfacial tension

In theory, a transient interfacial tension can exist across the boundary of any two fluids with unequal chemical potentials even if these fluids are completely miscible, and a simple Fickean model gives that this interfacial tension should decay as $t^{-1/2}$ owing to interdiffusion across the interface. Recently, Smith, van de Ven, and Mason[13] measured the interfacial tension between two mutually miscible silicone oils and showed that it indeed decayed with time, although these investigators could not document the predicted $t^{-1/2}$ dependence.

Let us suppose that the effect of the interfacial tension may not be negligible in our experiments. At first, this assumption seems to contradict the results presented in Sec. II B where a depression forming at the rear stagnation point of an oblate spheroid was found to grow without bound only if the interfacial tension was negligibly small. However, recall that in the theoretical development we did not take into account the tail emanating from the rear stagnation point, and it may be argued that the presence of the tail leads to a local convexity of the surface as seen from within the drop which, if the interfacial tension is nonzero, creates a positive external capillary pressure, thereby causing the external fluid to cave in. It is then plausible that even in the presence of a finite interfacial tension, a depression still forms and grows near the rear stagnation point of the drop.

Returning to the case of toroidal drops, we propose to back-calculate the values of γ which will remove the discrepancy between theory and experiments; in the computation we set $S_2 = 0$, since the drop cross section on the film does not appear to be distorted along the 45° axis, and consider only the first and the third terms on the right-hand side of Eq. (29′). The resulting values of γ are listed in Table IV in order of decreasing settling speed of the drop. We note immediately that the maximum value of γ is found in the run with the highest drop settling speed and correspondingly, that the minimum value of γ is associated with the slowest settling drop. This pattern is entirely consistent with the work of Smith *et al.*[13] and in fact the magnitudes of γ reported above are comparable to those in their paper.

It would be desirable to have an independent check to test whether or not the aforementioned discrepancy is due to the presence of the transient interfacial tension by, say, conducting the experiments in a system which would be expected to have a vanishingly small interfacial tension; in other words, we wish to minimize $\gamma/\mu U$. However, since γ decays

TABLE IV. Computed values of the interfacial tension.

Measured speed range cm/sec	System	Interfacial tension mN/m
0.90–1.07	3[a]	0.23
0.86–1.02	2	0.18
0.88–0.98	1	0.18
0.81–0.91	4[b]	0.16
0.74–0.84	3[a]	0.12
0.40–0.45	4[b]	0.02
0.34–0.41	5	0.03
0.26–0.34	6	0.02

[a, b] Different size drops used.

with time in a system consisting of two distinct miscible fluids, small values of γ are achieved only at low U, and thus it does not seem possible to reduce $\gamma/\mu U$ significantly.

We avoided this difficulty by using the same fluid for the drop as that of the bulk medium but at a sufficiently low temperature such that the resulting density difference was large enough for the drop to fall in the continuum under the force of gravity. Under these conditions, the effect of the interfacial tension should be negligible, since the authors are unaware of reports in the literature which suggest that a time-dependent interfacial tension exists between two identical fluids having different temperatures. The drops, initially at their freezing point, were formed just above the free surface and were allowed to enter the bulk fluid which was at 21 °C. A typical transient deformation of such a drop is shown in Fig. 8. As before, the drop entering the bulk medium left behind a tail emanating from the rear stagnation point where a depression formed. This depression deepened, but here the manner of growth was distinct from the case in which the fluid comprising the drop had a composition that differed from that of the ambient fluid. Instead of deepening primarily along the axis of symmetry, the depression spread so that the drop eventually deformed into a hollow spherical cap (Fig. 8), by which time significant heat transfer seemed to have occurred, thereby reducing the density difference, so that the drop became stagnant. In our laboratory, the drop under these conditions was seen to deform into a ring rather than a spherical cap only once. In contrast, when the above procedure was repeated with two fluids of different compositions, a torus formation was always observed. To be sure, the rate of heat transfer from a ring should be considerably lower than that from a thin film shaped in the form of a hollow spherical cap, and the difference in the nature of drop deformation is due not only to the varying magnitudes of the interfacial tension but also to the effect of heat transfer. Nevertheless, in the initial stages of deformation where the drop is approximately spherical, it is reasonable to postulate that the rates of heat transfer are comparable in the two cases, and it appears that the formation of a hollow spherical cap is possible only if the interfacial tension is negligibly small.

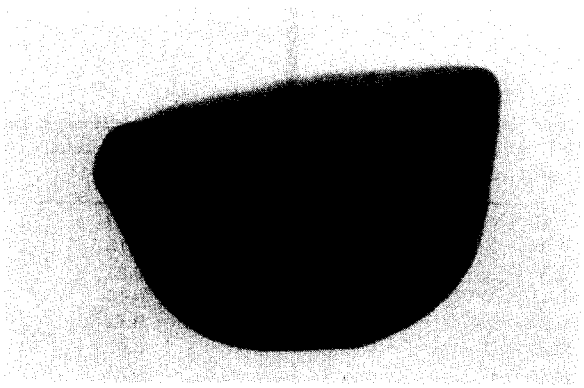

FIG. 8. Sideview photograph of a hollow spherical cap at 21 °C. Initial drop temperature is approximately − 7 °C.

D. Ring instability

Before concluding, it would be appropriate to give a brief and qualitative description of drop breakup as observed in our systems, and also to comment on the similarities between the instabilities of laminar vortex rings and of viscous rings at low Reynolds numbers. It was found that as a viscous ring expanded, the instability developed in the form of an azimuthal asymmetry whereby two crests and corresponding troughs formed out of the plane of the ring (see Fig. 4). As in the case of vortex rings,[14] the crests did not travel around the ring, and in addition the number of crests seemed to increase with increasing Reynolds number; for example, three crests appeared at $R_b \sim 1$. Following the first breakup of the ring, two additional "rings," although not closed, formed from the troughs, and they in turn underwent further instabilities. In contrast, such a repeating instability of a laminar vortex ring has rarely been observed because the azimuthal velocity induced by the instability appears to have a stabilizing effect on the resulting turbulent ring.

Finally, the behavior of two viscous rings with their axes of symmetry close to each other and at some vertical distance apart was identical to the leapfrogging of coaxial circular vortex filaments in that the rear ring approached the front ring with increasing speed, and eventually passed through it. In our laboratory, this process was observed to repeat itself up to three times before the rings disintegrated. Furthermore, leapfrogging occurred even when the axes of the viscous rings were at an angle to each other, in contrast to the case of vortex rings where this phenomenon is observed only if they are exactly coaxial.

ACKNOWLEDGMENTS

This research was supported in part by the National Science Foundation (Grant No. MEA 81-21713) and by the U. S. Department of Energy (Contract No. DOE AT03-80-ER10659.

[1] R. L. Powell and S. G. Mason, AIChE J. **28**, 286 (1982).
[2] R. G. Cox, J. Fluid Mech. **37**, 601 (1969).
[3] S. Torza, R. G. Cox, and S. G. Mason, J. Colloid Interface Sci. **38**, 395 (1972).
[4] T. D. Taylor and A. Acrivos, J. Fluid Mech. **18**, 466 (1964).
[5] Y. Matunobu, J. Phys. Soc. Jpn. **21**, 1596 (1966).
[6] Masami Kojima, Ph.D. dissertation, Stanford University, 1983.
[7] H. K. Moffatt and D. W. Moore, J. Fluid Mech. **87**, 749 (1978).
[8] R. E. Johnson and T. Y. Wu, J. Fluid Mech. **95**, 263 (1979).
[9] I. Proudman and J. R. A. Pearson, J. Fluid Mech. **2**, 237 (1957).
[10] J. Happel and H. Brenner, *Low Reynolds Number Hydrodynamics* (Prentice-Hall, Englewood Cliffs, NJ, 1965).
[11] H. Brenner and R. G. Cox, J. Fluid Mech. **17**, 561 (1963).
[12] A. M. D. Amarakoon, R. G. Hussey, B. J. Good, and E. G. Grismal, Phys. Fluids **25**, 1495 (1982).
[13] P. G. Smith, T. G. M. van de Ven, and S. G. Mason, J. Colloid Interface Sci. **80**, 302 (1980).
[14] T. Maxworthy, J. Fluid Mech. **81**, 465 (1977).